CHIN. PHYS. LETT. Vol. 36, No. 1 (2019) 017301

Spin Caloritronic Transport of Tree-Saw Graphene Nanoribbons *

Yu-Zhuo LV(吕钰卓), Peng ZHAO(赵朋)**

School of Physics and Technology, University of Jinan, Jinan 250022

(Received 13 August 2018)

Using density functional theory combined with non-equilibrium Green's function method, we investigate the spin caloritronic transport properties of tree-saw graphene nanoribbons. These systems have stable ferromagnetic ground states with a high Curie temperature that is far above room temperature and exhibit obvious spin-Seebeck effect. Moreover, thermal colossal magnetoresistance up to 10^{20}% can be achieved by the external magnetic field modulation. The underlying mechanism is analyzed by spin-resolved transmission spectra, current spectra and band structures.

PACS: 73.23.−b, 85.65.+h, 71.15.Mb DOI: 10.1088/0256-307X/36/1/017301

Spin caloritronics, which focuses on the interplay of spin and heat transport in materials, has attracted great attention because it offers potential applications in thermoelectric waste heat recovery and information-processing technologies.[1−4] The concept of spin caloritronics can be traced back to the late-1980s with Johnson and Silsbee's investigations of non-equilibrium thermodynamics of spin, charge and heat in metallic heterostructures.[5,6] However, this field only grew after the experimental observation of spin-Seebeck effect (SSE) in 2008 by Uchida *et al.* in ferromagnetic metal NiFe alloy.[7] In SSE, the spin-up and spin-down currents flowing in opposite directions, as well as the associated spin voltage are induced by a temperature gradient, which lays the foundation for applying spin caloritronics in the energy-saving devices.

Recent studies have shown that graphene nanoribbons (GNRs) have strong potential for spin caloritronics. For example, Zeng *et al.* explored the thermally induced spin transport properties of zigzag GNRs (ZGNRs), and observed SSE, thermal spin-filtering and thermal magnetoresistance effects.[8] Ni *et al.* found the SSE and thermal colossal magnetoresistance effects in a ZGNR heterojunction with a single-hydrogen-terminated ZGNR as the left electrode and a double-hydrogen-terminated ZGNR as the right electrode.[9] Huang *et al.* reported ZGNR co-doped with nitrogen and boron atoms exhibits excellent thermal spin transport properties.[10] Tang *et al.* designed a kind of armchair GNRs (AGNR) with special edge hydrogenation, and found SSE and spin-Seebeck diode effects.[11] Recently, Yu *et al.* proposed two kinds of novel GNRs with sawtooth edges: tree-saw GNRs (TGNRs) and Christmas-tree GNRs (CGNRs).[12] They found that both TGNRs and CGNRs exhibit ferromagnetic (FM) ground states. Especially, TGNRs have more stable FM ground states, which portends much higher Curie temperature and potential applications in the field of spin caloritronics.

In the present work we use the density functional theory (DFT) in conjunction with non-equilibrium Green's function (NEGF) technique and explore the spin caloritronic transport properties of TGNRs. Our results show that obvious SSE can be generated in these systems. Moreover, with the help of external magnetic field modulation, a thermal colossal magnetoresistance of up to 10^{20}% can be achieved.

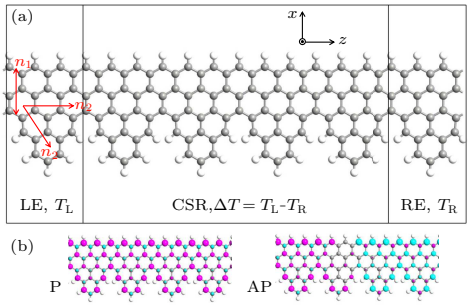

Fig. 1. (a) Schematic of the TGNR-based spin caloritronic device, which is divided into three parts: left electrode (LE), central scattering region (CSR) and right electrode (RE). Two integers (n_1, n_2) indicate the size of TGNR primitive cell, T_L and T_R are the electron temperature of LE and RE, and $\Delta T = T_L - T_R$ is the temperature difference. (b) Spin density distribution across the CSR for the P and AP configurations, where the pink and cyan colors denote the spin-up and spin-down components, respectively.

We adopt two integers (n_1, n_2) to characterize the size of TGNR primitive cell, where n_1 is the number of continuous zigzag carbon chains, and n_2 is the number of hexagonal rings along the n_2 direction (see Fig. 1(a)), respectively. Figure 1(a) plots the TGNR-based spin caloritronic device with $n_1 = n_2 = 3$, which is labeled as T(3,3) for simplicity. The integer $n_2 = 3$ for TGNRs corresponds to the lowest numbers meeting the requirement of the sawtooth edges.[12] Our test shows that the TGNRs with larger n_1 or n_2 present similar results, thus we focus on T(3,3). As shown in Fig. 1(a), the entire device consists of left electrode (LE), central scattering region (CSR) and right elec-

*Supported by the Natural Science Foundation of Shandong Province under Grant No ZR2016AM11.
**Corresponding author. Email: ss_zhaop@ujn.edu.cn
© 2019 Chinese Physical Society and IOP Publishing Ltd

trode (RE). The electrodes and CSR are represented by one and four T(3,3) primitive cells along the transport (z) direction, respectively. Our test shows that the longer CSR gives similar results. Large enough vacuum layers in the x (25 Å) and y (20 Å) directions are added to eliminate the interaction between adjacent ribbons.

Our calculations are all performed by the Atomistix Toolkit (ATK) package,[13–16] which is based on the DFT+NEGF method. Structural relaxation is carried out for the TGNR primitive cell until the residual force on each atom is less than 0.01 eV/Å and the total energy is converged to 10^{-5} eV. The spin generalized gradient approximation with Perdew–Burke–Ernzerhof form of functions (SGGA.PBE) is employed for the exchange-correlation potential.[17] The core electrons are described by Troullier–Martins norm-conserving pseudopotentials,[18] while the valence electron wave functions are expanded by double-zeta plus polarization (DZP) basis set. The real space grid technique is used with the energy cutoff of 200 Ry in numerical integration. The k-point grids 1, 1 and 100 are adopted in the x, y and z directions, respectively. The thermal spin currents flow through the device are calculated by the Landauer–Büttiker formula[19] $I_\sigma = (e/h)\int_{-\infty}^{\infty} T_\sigma(E)[f_{\rm L}(E,T_{\rm L}) - f_{\rm R}(E,T_{\rm R})]{\rm d}E$, where e is the electron charge, h is Planck's constant, $T_\sigma(E)$ is the transmission function of carriers with energy E and spin index σ (σ=up and dn for spin-up and spin-down), and $T_{\rm L/R}$ and $f_{\rm L/R}$ are the temperature and Fermi-Dirac distribution function of LE/RE, respectively.

To study the magnetic ground state, three different magnetic states, FM state, antiferromagnetic (AFM) state, and non-magnetic (NM) state are considered. We use the labels $E_{\rm FM}$, $E_{\rm AFM}$ and E_{NM} to denote the total energies per primitive cell for the FM, AFM and NM states of T(3,3), respectively. The calculated energy differences $E_{\rm AFM} - E_{\rm FM} = 130.74$ meV and $E_{NM} - E_{\rm FM} = 262.13$ meV, indicating that the FM state is the ground state. Using the mean field theory, the Curie temperature ($T_{\rm C}$) is estimated,[20] namely, $E_{\rm AFM} - E_{\rm FM} = \gamma k_{\rm B} T_{\rm C}/2$, where γ and $k_{\rm B}$ represent the dimension of the system ($\gamma = 1$ for one-dimensional TGNR system) and the Boltzmann constant, respectively. We then obtain a $T_{\rm C}$ up to 3029 K, which is far above room temperature and indicates that TGNRs are potential materials for spin caloritronic devices.

Because the magnetization of electrodes can be controlled by applying external magnetic fields, two distinct magnetic configurations are considered: parallel (P) and anti-parallel (AP) configurations.[21–23] To be specific, for the P configuration, no external magnetic field is needed due to the high $T_{\rm C}$, while for the AP configuration, external magnetic fields at two electrodes pointing in opposite ($+y$, $-y$) directions are needed. Figure 1(b) plots the spin density ($\Delta\rho = \rho_{\rm up} - \rho_{\rm dn}$) distribution across the CSR for the P and AP configurations, where the pink and cyan colors denote the spin-up and spin-down components, respectively. Evidently, the spin density distribution verifies two magnetic configurations setups: the whole CSR are spin-up polarized under the P configuration, while the left and right regions of CSR are spin-up and spin-down polarized under the AP configuration, respectively.

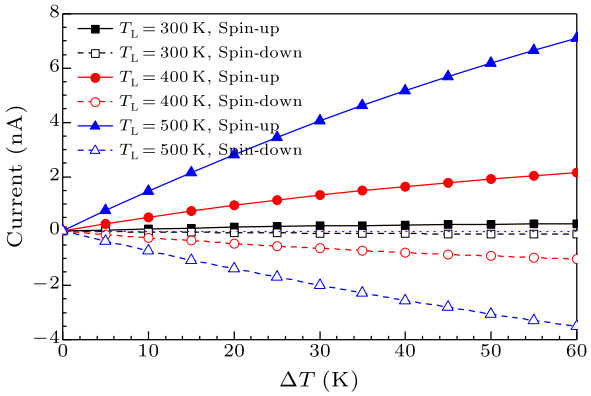

Fig. 2. Calculated thermal spin currents versus ΔT with $T_{\rm L} = 300$, 400 and 500 K.

We first consider the P configuration. Figure 2 plots the calculated thermal spin currents versus temperature difference (ΔT) between two electrodes, i.e., $\Delta T = T_{\rm L} - T_{\rm R}$, with $T_{\rm L}$ varying from 300 to 500 K. As one can see, the spin-up ($I_{\rm up}$) and spin-down ($I_{\rm dn}$) currents are positive and negative, respectively, indicating that they flow in opposite directions. This is an obvious SSE because both $I_{\rm up}$ and $I_{\rm dn}$ are induced by temperature gradient rather than by bias gradient. Moreover, both $I_{\rm up}$ and $I_{\rm dn}$ are very weak when $T_{\rm L} = 300$ K, and both of them increase with $T_{\rm L}$ or ΔT.

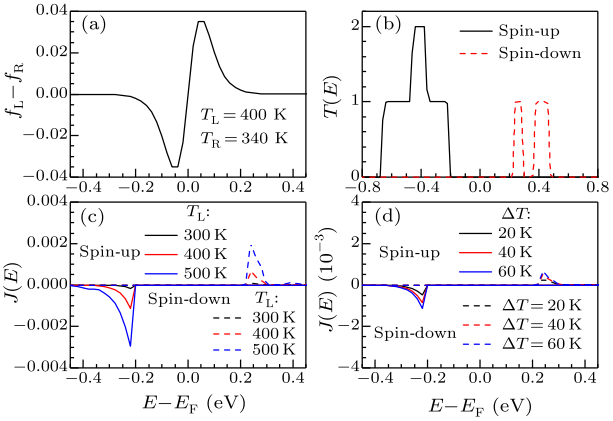

Fig. 3. (a) Difference in Fermi–Dirac distribution function of two electrodes, ($f_{\rm L} - f_{\rm R}$), with $T_{\rm L} = 400$ K and $T_{\rm R} = 340$ K. (b) Spin-resolved transmission spectra. (c) Spin-resolved current spectra for fixed $\Delta T = 60$ K with $T_{\rm L} = 300$, 400 and 500 K. (d) Spin-resolved current spectra for fixed $T_{\rm L} = 400$ K with $\Delta T_{\rm L} = 20$, 40 and 60 K.

According to the Landauer–Büttiker formula, the thermal spin currents are the joint results of T_σ and $f_{\rm L} - f_{\rm R}$. To clarify the underlying mechanism of the

observed SSE, we first consider $f_L - f_R$, which is dependent on T_L and T_R since two electrodes are composed of the same material. Figure 3(a) plots $f_L - f_R$ with $T_L = 400\,K$ and $T_R = 340\,K$ as a function of $E - E_F$, where E_F is the Fermi level. As can be seen, $f_L - f_R < 0$ or > 0 when $E < E_F$ or $E > E_F$, indicating that both the hole and electron carrier concentrations in LE are higher than those in RE. Consequently, both hole and electron carriers diffuse from the hot LE to the cold RE, leading to a positive hole current I_h and a negative electron current I_e in the opposite direction. Moreover, as shown in Fig. 3(a), $f_L - f_R$ is perfect symmetric with respect to E_F, and it also exhibits a typical exponential decaying nature characteristics. Thus, only the transmissions close to E_F have contribution to the thermal current. However, I_h and I_e will cancel out each other if the transmissions around E_F are also symmetry. Figure 3(b) plots the spin-resolved transmission spectra. Clearly, both T_{up} and T_{dn} are asymmetric about E_F. Specifically, a broad spin-up transmission band lies in the energy region $-0.68\,eV < E - E_F < -0.2\,eV$, while two narrow spin-down transmission bands lie in the energy regions of $0.22\,eV < E - E_F < 0.3\,eV$ and $0.36\,eV < E - E_F < 0.48\,eV$, respectively. Therefore, nonzero net thermal current can be obtained due to the break of electron-hole symmetry. To further understand the combined effects of T_σ and $f_L - f_R$ on the thermal spin currents, as shown in Figs. 3(c) and 3(d), we plot the spin-resolved current spectra $J_\sigma = T_\sigma(f_L - f_R)$ as a function of $E - E_F$. Figure 3(c) corresponds to J_σ for fixed $\Delta T = 60\,K$ with $T_L = 300$, 400 and 500 K. Figure 3(d) corresponds to J_σ for fixed $T_L = 400\,K$ with $\Delta T = 20$, 40 and 60 K. Evidently, as shown in Figs. 3(c) and 3(d), the peaks of J_{up} and J_{dn} occur below and above E_F, giving rise to positive I_{up} and negative I_{dn}. Moreover, the magnitude of thermal spin currents is determined by the cover area of J_σ according to the Landauer–Büttiker formula. As shown in Fig. 3(c), both the cover areas of J_{up} and J_{dn} are very small when $T_L = 300\,K$, leading to the very weak I_{up} and I_{dn}. As T_L goes up, both the cover areas of J_{up} and J_{dn} increase obviously, resulting in the significant increases of I_{up} and I_{dn}. Similarly, as shown in Fig. 3(d), both the cover areas of J_{up} and J_{dn} increase with ΔT, resulting in the gradual increases of I_{up} and I_{dn}.

The origin of transmission bands around E_F can be elucidated by the spin-resolved band structures of two electrodes. Figure 4(a) plots the spin-resolved band structures of LE (left panel) and RE (right panel), as well as the spin-resolved transmission spectra (middle panel). Clearly, the band structures of LE are the same as those of RE under the P configuration since two electrodes are composed of the same material. Around E_F, two spin-up bands V_1 and V_2 appear in energy region $-0.68\,eV < E - E_F < -0.36\,eV$ and $-0.46\,eV < E - E_F < -0.2\,eV$, while two spin-down bands C_1 and C_2 appear in the energy regions $0.22\,eV < E - E_F < 0.3\,eV$ and $0.36\,eV < E - E_F < 0.48\,eV$, respectively. The perfect overlapping of V_1, V_2, C_1 and C_2 between LE and RE causes the spin-resolved transmission bands around E_F.

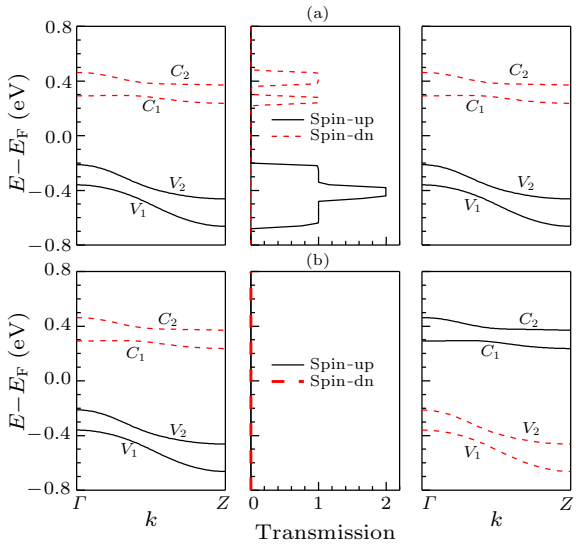

Fig. 4. Spin-resolved band structures of LE (left panel) and RE (right panel), as well as the spin-resolved transmission spectra (middle panel) under (a) P and (b) AP configurations.

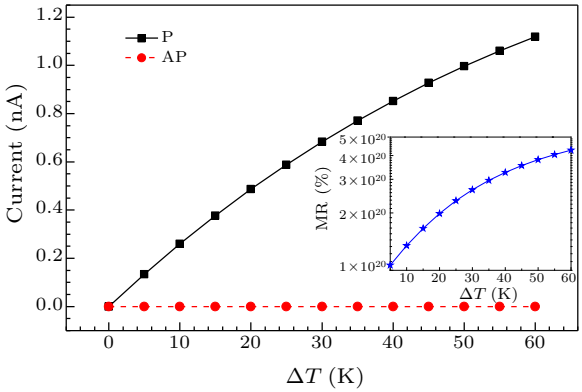

Fig. 5. Total thermal current under the P and AP configurations for fixed $T_L = 400\,K$ with different ΔT. The inset shows the magnetoresistance ratio (MR) as a function of ΔT with fixed $T_L = 400\,K$.

Next, we consider the AP configuration. Figure 4(b) plots the spin-resolved band structures of LE (left panel) and RE (right panel), as well as the spin-resolved transmission spectra (middle panel) under the AP configuration. As we can see, C_1, C_2 and V_1, V_2 in RE are now spin-up and spin-down bands, which are exactly interchanged compared with those in LE. Thus, a large transmission gap around E_F occurs due to the lack of overlapping between bands with the same spin index. As a result, I_{up} and I_{dn} can hardly pass through the device under the AP configuration. Figure 5 plots the total thermal current $(I_{up} + I_{dn})$ under the P (I_P) and AP (I_{AP}) configurations for fixed $T_L = 400\,K$ with different ΔT. Clearly, obvious I_P can flow through the device while I_{AP} is strongly blocked, resulting in a thermal colossal magnetoresistance effect when the magnetic configuration goes from P to

AP. To quantify the predicted thermal colossal magnetoresistance effect, we define the magnetoresistance ratio (MR) as $\mathrm{MR} = [(|I_{\mathrm{P}}| - |I_{\mathrm{AP}}|)/|I_{\mathrm{AP}}|] \times 100\%$. As shown in the inset of Fig. 5, MR is as large as $10^{20}\%$ and increases gradually with ΔT. This large MR is much greater than those reported previously.[8,9]

In conclusion, we have investigated the spin caloritronic transport properties of TGNRs using the DFT+NEGF method. Our results show that TGNRs have stable FM ground states with high T_{C} far above room temperature. Under the P configuration, these systems exhibit obvious SSE due to the break of electron-hole symmetry originated from the asymmetry of spin-resolved transmission spectra around E_{F}. Moreover, large thermal colossal magnetoresistance of up to $10^{20}\%$ can be realized when the magnetic configuration switches between P and AP. These results demonstrate that TGNRs hold great potential for spin caloritronics.

References

[1] Goennenwein S T B and Bauer G E W 2012 *Nat. Nanotechnol.* **7** 145
[2] Bauer G E W, Saitoh E and van Wees B J 2012 *Nat. Mater.* **11** 391
[3] Jeon K R, Min B C, Spiesser A, Saito H, Shin S C, Yuasa S and Jansen R 2014 *Nat. Mater.* **13** 360
[4] Chang P H, Bahramy M S, Nagaosa N and Nikolić B K 2014 *Nano Lett.* **14** 3779
[5] Johnson M and Silsbee R H 1987 *Phys. Rev. B* **35** 4959
[6] Johnson M and Silsbee R H 1988 *Phys. Rev. B* **37** 5326
[7] Uchida K, Takahashi S, Harii K, Ieda J, Koshibae W, Ando K, Maekawa S and Saitoh E 2008 *Nature* **455** 778
[8] Zeng M, Feng Y and Liang G 2011 *Nano Lett.* **11** 1369
[9] Ni Y, Yao K, Fu H, Gao G, Zhu S and Wang S 2013 *Sci. Rep.* **3** 1380
[10] Huang H, Zheng A, Gao G and Yao K 2018 *J. Magn. Magn. Mater.* **449** 522
[11] Tang X Q, Ye X M, Tan X Y and Ren D H 2018 *Sci. Rep.* **8** 927
[12] Yu D, Lupton E M, Gao H J, Zhang C and Liu F 2008 *Nano Res.* **1** 497
[13] Taylor J, Guo H and Wang J 2001 *Phys. Rev. B* **63** 121104(R)
[14] Taylor J, Guo H and Wang J 2001 *Phys. Rev. B* **63** 245407(R)
[15] Brandbyge M, Mozos J L, Ordejón P, Taylor J and Stokbro K 2002 *Phys. Rev. B* **65** 165401
[16] Soler J M, Artacho E, Gale J D, García A, Junquera J, Ordejón P and Sánchez-Portal D 2002 *J. Phys.: Condens. Matter* **14** 2745
[17] Perdew J P, Burke K and Ernzerhof M 1996 *Phys. Rev. Lett.* **77** 3865
[18] Troullier N and Martins J 1991 *Phys. Rev. B* **43** 1993
[19] Büttiker M, Imry Y, Landauer R and Pinhas S 1985 *Phys. Rev. B* **31** 6207
[20] Zhang J, Li X and Yang J 2014 *Appl. Phys. Lett.* **104** 172403
[21] Kim W Y and Kim K S 2008 *Nat. Nanotechnol.* **3** 408
[22] Cho W J, Cho Y, Min S K, Kim W Y and Kim K S 1993 *J. Am. Chem. Soc.* **115** 9389
[23] Zhang Y T, Jiang H, Sun Q F and Xie X C 2010 *Phys. Rev. B* **81** 165404